

# Blind Image Restoration Based on $l_1 - l_2$ Blur Regularization

Su Xiao

**Abstract**—Improving the quality of reconstructed images in blind image restoration tasks remains a challenging and important problem. To solve this problem, a new methodology is proposed based on sparse representation and regularization. In this method, blind image restoration is divided into two steps: blur estimation and high-quality image reconstruction. In the blur estimation step, a new sparse regularized blur estimation model is built; it uses the  $l_1$  norm of the gradient image and the  $l_1 - l_2$  mixed norm of the blur kernel as the regularization terms. The variable splitting method is applied to the sparse regularized blur estimation model to perform an equivalent model transformation; alternating minimization is then utilized to decompose the equivalent model into several simpler sub-problems. As a result, the blur kernel estimate can be obtained with an alternating estimation approach for the subproblems by using a fast Fourier transform, soft-thresholding iteration, etc. To improve the accuracy, a multiscale strategy is integrated into the iterative estimation process of the blur kernel, and the model parameters are updated with a continuous method. In the clear image reconstruction stage, the image deconvolution problem in reconstruction is solved with a hyper-Laplacian sparse prior-based method. In the experiments, simulations are performed, and the results are compared with the results of two similar methods. In the experiment, famous synthetic blurred images and real-world blurred images from a public image library are used. The comparative results validate the effectiveness of the proposed method and demonstrate its effectiveness.

**Index Terms**—blind image restoration, sparse regularization, variable splitting, alternating minimization, soft-thresholding iteration.

## I. INTRODUCTION

WITH the popularization of social networks and the powerful multimedia capabilities of smartphones, images are playing an increasingly important role as multimedia information carriers. However, the quality of digital images has always been degraded by blurring and noise. To eliminate the adverse effects of image degradation, blind image restoration concepts and theories have been proposed since the 1960s and 1970s. With the complexity, variability, and unpredictability of the image degradation process, the blind image restoration problem has remained an actively investigated topic, and interesting and valuable solutions have been proposed. With years of research results, blind image restoration methods are inseparable from prior knowledge (hypothesis). As a result, accurate prior information for unknown clear images, unknown blur kernels, noise, etc. can undoubtedly improve the quality of blindly restored images. In recent years, new technologies and theories have been introduced to improve the quality of blind image restoration,

where the introduction of sparse representation technology is recognized as a classic method. Within the sparse representation framework, the prior knowledge of the image can be used to represent the image in a sparse way under a given transformation, such as gradients of images or coefficients under wavelet decomposition. Because the  $l_p$  ( $0 \leq p \leq 2$ ) norm can be used to measure the sparseness of signals, the  $l_p$  norm can be naturally used to induce the sparsity of the solution. In recent years, excellent sparsity-driven blind image restoration methods have been proposed by incorporating regularization, variational Bayesian, and other techniques in which variable splitting, alternating optimization, a Bregman iteration, etc. are widely used.

Babacan et al. [1] proposed a blind image restoration method based on a Bayesian inference and hyper-Gaussian sparsity prior to overcoming the drawbacks of the conventional maximum a posteriori approach. However, the authors only considered the prior models of the Gaussian image; they recognized that other prior models could lead to further improvements in the efficiency of blind image restoration. Under the Bayesian framework, Amizic et al. [2] proposed a novel blind restoration method for images based on an image with a sparse prior with an  $l_p$  norm and a blur prior with a total variation norm. In this case, a majorization-minimization method was adopted to perform a Bayesian inference and obtain the maximum a posteriori result of the unknown image and the unknown blur and model parameters. Because total variation regularization can effectively restore the edges of an image, Li et al. [3] extended the standard total variation model to the blind image restoration problem, and the extended split Bregman method was used to iteratively solve the minimization problem caused by restoration. Clear images with a simple or complex background were successfully restored with low computational complexity. By utilizing a Bayesian inference and convex analysis, Zhang et al. [4] proposed a spatially adaptive sparse image regularization and blind restoration method. Based on an implicit normalization process, the form of the regularization term was automatically adapted to match the estimated degree of local blur and the image structure. Therefore, a key advantage of this approach is the avoidance of parameter tuning. The success of image restoration with the maximum a posteriori estimation partly comes from the respective intermediate steps, which implicitly or explicitly reconstruct an unnatural image with a significant structure. Based on this approach, Xu et al. [5] adopted the “unnatural”  $l_0$  norm to perform a kernel estimation and large-scale optimization, where the gradient sparsity of  $l_0$  eliminates the harmful small-amplitude structures. The proposed method not only provides a principled understanding of efficient blind image restoration but also significantly improves optimization performance. To perform a satisfactory blur kernel

Manuscript received July 1, 2019; revised September 21, 2019. This work was supported by the Natural Science Research Project of the Education Department of Anhui Province under Grant KJ2018A0397.

Su Xiao is with the School of Computer Science and Technology, Huaibei Normal University, Huaibei, Anhui Province, 235000 China. e-mail: csxiaosu@139.com.

estimation, a maximum a posteriori estimation-based blind image restoration usually depends on well-designed regularization operators and manual parameter tuning. Various regularization operators can reflect the smoothness of the structure but are unable to enhance the edges. Therefore, in the MAP framework, Zuo et al. [6] proposed a method to solve the edge enhancement problem with an iterative  $l_p$  norm sparse regularization operator and a data-driven strategy. The generalized shrinkage-thresholding operator was first extended to suppress fine details and enhance edges. Subsequently, an iterative generalized contraction-thresholding operator parameter was specified for dynamic edge selection and time-varying regularization. Finally, the principle discriminant learning method was used to learn the iterative generalized shrinkage-thresholding operator from the training data. Cai et al. [7] proposed a blind restoration method based on sparse regularization. The sparse modeling of clear images and blur kernels was performed within the tight wavelet framework. The improved split Bregman method was also used to optimize the restoration. In an alternative research direction, the problem of obtaining satisfactory results without prior information related to the blur kernel has been investigated. Pan et al. [8] proposed a simple and effective  $l_0$  regularization prior based on the intensity and gradient for the blind restoration of text images. Based on this prior, an efficient optimization method was proposed to obtain reliable intermediate results for blur kernel estimation. In this method, no complicated filtering strategy was required to select the edges. In the final clear image reconstruction step, a simple method was proposed to eliminate artifacts and obtain the desired results. With a dual  $l_0 - l_2$  norm sparse regularization approach, Shao et al. [9] proposed a simple and fast estimation method by alternately using the coupling operator splitting method and the augmented Lagrangian method to identify the clear image portions and blur kernels, respectively. In the final clear image reconstruction step, a simple method was designed to eliminate artifacts and achieve the desired results. In [10], Yan et al. observed that bright channel pixels were bright long after the blurring process, and an extreme channel prior-based blind image restoration method was proposed with sparse  $l_0$  norm regularization. In particular, this approach combined the advantages of the bright channel prior and the dark channel prior, where the method of semi-quadratic splitting was utilized. According to the blind restoration of sparsely optimized images, this paper proposes the application of  $l_1 - l_2$  dual regularization for the blur kernel. Based on this method, a new sparse regularization model is constructed that adopts variable splitting, alternating minimization, a fast Fourier transform, soft threshold iteration, and other methods to process images and obtain the best estimate of the blur kernel. To improve the accuracy of blur estimation, the blur kernel estimation and parameter updating strategies are carefully selected and integrated into the iterative process. In the stage of clear image reconstruction, image deconvolution is performed by using the mature and effective super-Laplacian prior method proposed by Krishnan et al. [11].

## II. BLUR ESTIMATION MODEL AND ITS SOLUTION

Let  $k$  and  $x$  denote the unknown blur kernel and clear image, respectively.  $y$  denotes the observed blurred image,

and  $n$  denotes the additive noise. Thus, the image degradation process can be expressed as

$$y = k \otimes x + n, \quad (1)$$

where  $\otimes$  denotes a convolution operation. Because convolution is a linear operation, Equation (1) can be expressed as

$$\nabla y = k \otimes \nabla x + n, \quad (2)$$

where  $\nabla$  denotes a gradient operation, and  $\nabla y$  and  $\nabla x$  denote the gradient images of  $x$  and  $y$ , respectively. Obviously, the purpose of blur estimation is to obtain the best estimate of  $k$  through  $y$  (or  $\nabla y$ ). Compared with Equation (1), the degradation model shown in Equation (2) usually provides an accuracy improvement for blur estimation [12].

Under the regularization framework, the blur estimation problem can be expressed as

$$\min_{x,k} \frac{1}{2} L(k, x) + R_1(x) + R_2(k), \quad (3)$$

where  $L(k, x)$  is a reliability term. In the linear system of Equation (2),  $L(k, x) = \frac{1}{2} \times \|\nabla y - k \otimes \nabla x\|_2^2$ ,  $\|\cdot\|_2$ , i.e., the  $l_2$  norm. Moreover,  $R_1(x)$  and  $R_2(k)$  are the regularization terms. In the sparse representation framework, these terms are usually the  $l_p$  ( $0 \leq p \leq 2$ ) norms or are given by a mixed representation.

Considering the sparsity of the gradient image, let  $R_1(x) = \alpha \|\nabla x\|_1$ , where  $\|\cdot\|_1$  is the  $l_1$  norm. Additionally, considering the sparseness of the blur kernel and its composition of edges and smooth regions, let  $R_2(k) = \beta \|k\|_1 + \gamma \|k\|_2^2$ . The  $l_1$ -regularization term can be used to ensure that the blur estimation is sparse, and the  $l_2$ -regularization term can accurately reconstruct the smooth region of the blur kernel by eliminating isolated points. Accordingly, the blur estimation model based on the sparse regularization established in this paper can be expressed as

$$\min_{k,u} \frac{\|g - k \otimes u\|_2^2}{2} + \alpha \|u\|_1 + \beta \|k\|_1 + \frac{\gamma}{2} \|k\|_2^2, \quad (4)$$

where  $g = \nabla y$ ,  $u = \nabla x$ , and  $\alpha$ ,  $\beta$ , and  $\gamma$  are positive constants.

Equation (4) shows the multivariate minimization task, and the objective function is non-differentiable due to the existence of the  $l_1$  norm. To avoid directly processing problem (4), the variable splitting method is used to obtain the equivalent transformation:

$$\min_{k,u,v,w} \frac{\|g - k \otimes u\|_2^2}{2} + \alpha \|v\|_1 + \beta \|w\|_1 + \frac{\gamma}{2} \|k\|_2^2, \quad (5)$$

s.t.  $v = u, w = k,$

where  $v$  and  $w$  are the introduced relaxation variables. Variable splitting is a convenient method that is widely used. The purpose of introducing new variables is to make multivariate non-differentiable optimization problems easier to solve.

Next, the application of an alternating minimization operation to Equation (5) yields the following expressions:

$$u^{m+1} = \arg \min_u \|g - k^m \otimes u\|_2^2 + \mu_1 \|v^m - u\|_2^2, \quad (6)$$

$$v^{m+1} = \arg \min_v \alpha \|v\|_1 + \frac{\mu_1}{2} \|v - u^{m+1}\|_2^2, \quad (7)$$

$$k^{m+1} = \arg \min_k \|g - k \otimes u^{m+1}\|_2^2 + \mu_2 \|w^m - k\|_2^2 + \gamma \|k\|_2^2, \quad (8)$$

$$w^{m+1} = \arg \min_w \beta \|w\|_1 + \frac{\mu_2}{2} \|w - k^{m+1}\|_2^2. \quad (9)$$

Alternating minimization embodies a “divide and conquer” concept. When addressing multiple unknowns, this method solves the optimization problem for one of the unknowns at a time, and the remaining unknown variables are fixed.

Each of the objective functions of the minimization problems in Equations (6) and (8) is quadratic differentiable. According to the Plancherel theory [13], the fast Fourier transform of a quadratic differentiable function is equal to the sum of the fast Fourier transform of each term, which can be directly used to solve the minimization problems in Equations (6) and (8):

$$u^{m+1} = F^{-1} \left( \frac{F^*(k^m)F(g) + \mu_1 F(v^m)}{F^*(k^m)F(k^m) + \mu_1} \right), \quad (10)$$

$$k^{m+1} = F^{-1} \left( \frac{F^*(u^{m+1})F(g) + \mu_2 F(w^m)}{F^*(u^{m+1})F(u^{m+1}) + \gamma + \mu_2} \right). \quad (11)$$

where  $F$  represents the fast Fourier transform,  $F^*$  represents the complex conjugate of  $F$ , and  $F^{-1}$  represents the inverse fast Fourier transform. Because Equation (7) and Equation (9) have separable structures, a soft-thresholding iteration method can be used to calculate  $v^{m+1}$  and  $w^{m+1}$  as follows:

$$v_l^{m+1} = \max(|u_l^{m+1}| - \frac{\alpha}{\mu_1}, 0) \frac{u_l^{m+1}}{|u_l^{m+1}|}, \quad (12)$$

$$w_l^{m+1} = \max(|k_l^{m+1}| - \frac{\beta}{\mu_2}, 0) \frac{k_l^{m+1}}{|k_l^{m+1}|}, \quad (13)$$

where  $v_l^{m+1}$ ,  $w_l^{m+1}$ ,  $u_l^{m+1}$  and  $k_l^{m+1}$  represent the  $l$ -th element of  $v^{m+1}$ ,  $w^{m+1}$ ,  $u^{m+1}$ , and  $k^{m+1}$ , respectively.

### III. BLUR ESTIMATION METHOD AND CLEAR IMAGE RECONSTRUCTION

Based on Equations (10) and (11), by combining necessary strategies and methods, the proposed methods are demonstrated in Fig. 1, and the corresponding description is given in **Method 1**.

---

#### Method 1 Proposed Method

---

**Input:**  $\alpha$ ,  $\beta$ ,  $\mu$ , and range of  $\mu_1$  and  $\mu_2$

**Input:**  $k_1$  (corresponding to  $g_1$ ),  $v$  and  $w$

**Output:** Final Estimate of blur kernel  $k_N^{M+1}$

- 1: **For**  $j = 1$  to  $N$  **do**
  - 2:     **For**  $m = 0$  to  $M$  **do**
  - 3:         According to Equation (10), calculate  $u^{m+1}$
  - 4:         According to Equation (11), calculate  $k_j^{m+1}$
  - 5:          $k_j^{m+1} = \frac{k_j^{m+1}}{\sum(k_j^{m+1})}$  and  $k_j^{m+1} = \text{abs}(k_j^{m+1})$
  - 6:          $\mu_1 = \mu_1 \times 2$ ,  $\mu_2 = \mu_2/2$
  - 7:     **EndFor**
  - 8:     Upsample from  $k_j^{M+1}$  to  $k_0^{j+1}$
  - 9: **EndFor**
- 

Because the actual size of the blur kernel is often unknown, a “coarse-to-fine” multiscale strategy [14] is incorporated into the blur estimation process to avoid the blur estimation from converging to a local minimum or local

maximum and to improve the estimation accuracy. This process updates the blur kernel according to a  $\{5 \times 5, 7 \times 7, 11 \times 11, 17 \times 17, 25 \times 25, 35 \times 35, 51 \times 51\}$  size sequence. To construct a multiscale strategy, the image pyramid  $g_j$  ( $1 \leq j \leq N$ ) is established based on the image  $g$ , where  $g_N = g$ ,  $g_j$  ( $1 \leq j \leq N - 1$ ) is sequentially downsampled by  $g$ . In the iterative process,  $g_j$  ( $1 \leq j \leq N$ ) corresponds to the blur kernel  $k_j^{m+1}$  ( $1 \leq j \leq N$ ). Moreover, the normalized constraint  $k_j^{m+1} = k_j^{m+1}/\sum(k_j^{m+1})$  and the non-negative constraint  $k_j^{m+1} = \text{abs}(k_j^{m+1})$  are applied to the blur kernel obtained in each iteration, which further improves the estimation accuracy. To promote the convergence of the iterative process and improve the efficiency under the premise of accuracy, the continuation method proposed in [15] is used to automatically update the parameters  $\mu_1$  and  $\mu_2$  in each iteration.

After obtaining the final estimate of the blur kernel, the blind image restoration problem becomes an image deconvolution problem (i.e., reconstructing a clear image). For such problems, many effective methods have been proposed in recent years. This paper uses a representative hyper-Laplacian prior method that deconvolves the image as a sparse regularization problem.

$$\min_x \lambda \|y - k \otimes x\|_2^2 + \|\nabla^h x\|_1^{\frac{2}{3}} + \|\nabla^v x\|_1^{\frac{2}{3}}, \quad (14)$$

where  $\nabla^h$  represents a gradient operation in the horizontal direction and  $\nabla^v$  represents a gradient operation in the vertical direction.

### IV. EXPERIMENTAL RESULTS

Experiments were conducted on a laptop with the following configuration: Windows 10 operating system, MATLAB R2012a emulation platform, i7-7700HQ CPU, and 16 GB memory. The experimental blurred images are from the image libraries provided by Levin et al. [16], Kohler et al. [17] and Lai et al. [18]; the image libraries provide well-known standard test images in the field of blind restoration. The experiments are divided into three groups, including the first group and the second group of quantitative experiments and the third group of qualitative experiments. To evaluate the performance of the proposed method, the methods developed by Pan et al. [11] and Yan et al. [14] are introduced and used for comparison. For the entire experiment, the parameters of the proposed method are set as follows:  $\alpha = 6 \times 10^{-2}$ ,  $\beta = 8 \times 10^{-3}$ ,  $\gamma = 2.5 \times 10^{-3}$ ,  $\mu_1 = [10^{-5} \ 10^5]$ ,  $\mu_2 = [10^5 \ 10^{-5}]$ , and  $M = 10$ . For Pan’s method and Yan’s method, the default settings are used.

**First Group of Quantitative Results.** The first group of experiments restores the blurred images in the Levin image library, and the clear images and blur kernels are shown in Fig. 2. The Levin image library contains four clear grayscale images, eight blur kernels with different sizes and shapes, and 32 blurred images. The blurred images are generated by using blurred kernels in otherwise clear images. Because the original clear images are known, the peak signal-to-noise ratio (PSNR) is used as an objective evaluation criterion for the quality of the restored image. Generally, when the PSNR value is higher, the quality of the restoration is higher. Because images are generated for each clear image, the PSNR averages obtained from the restoration

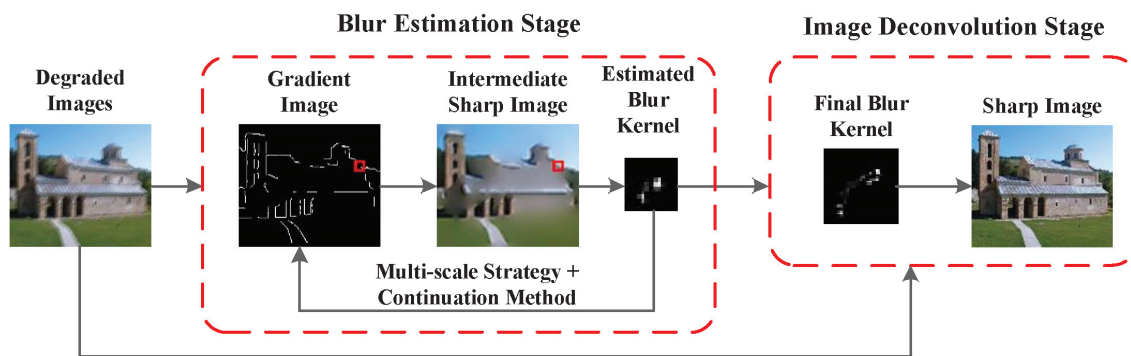


Fig. 1: Overall Process of the Proposed Method.

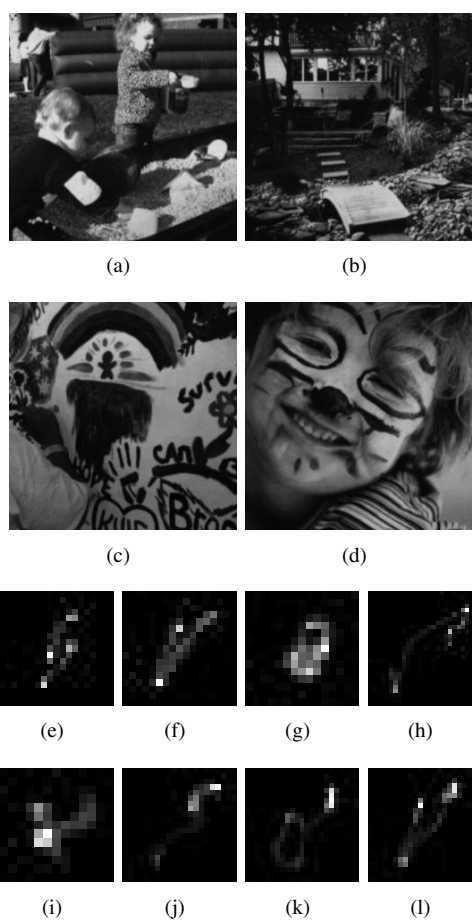


Fig. 2: Clear Images and Blur Kernels in the Levin Image Library. (a)-(d) Clear Images, and (e)-(l) Blur Kernels.

of the homologous eight blurred images are used to compare the restoration results of the respective methods. The average PSNR values obtained by the three methods are shown in Fig. 3, where P, Y and Pr represent the Pan's method, the Yan's method and the proposed method, respectively. The figure clearly indicates that the proposed method achieves the best recovery result, and the average for all of the PSNR values is the highest. To compare the accuracy of each method for blur kernel estimation, TABLE I records the average MSE values for the eight blur kernel estimates (smaller is better). Ker01 to Ker08 in TABLE I represent the blur kernels in Figs. 2(e) to 2(l). The estimation results in TABLE I clearly show that the proposed method has an advantage over other

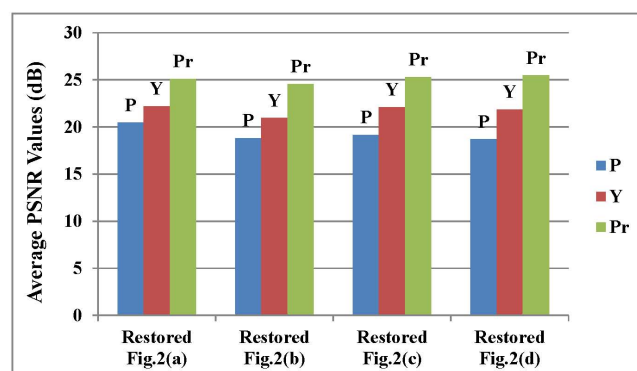


Fig. 3: Average PSNR Values for the Recovered Images in the Levin Image Library.

methods; that is, the proposed method can estimate the blur kernels more accurately, which contributes to improving the quality of blind image restoration.

**Second Group of Quantitative Results.** The images to be processed in the second group of experiments are shown in Fig. 4 and are from the public image library provided by Kohler et al. These images differ from the blurred versions of the same clear image. The images in this library are actually non-uniform blurred images, but they are still treated as uniform blurred images during the experiments. Because the original clear images are known, the experimental results are quantitatively analyzed, and the quantitative results are expressed by reconstructing the PSNR values of the clear image (larger is better). The quantitative results of the restored blurred image in Fig. 4 are reported in TABLES II and III, where dB is the unit of the PSNR values. As shown in Fig. 5, the actual visual effects of the reconstructed sharp images are also substantially consistent with the quantitative results. In the figure, the proposed method obtains clearer image details, while the other two methods reconstruct images with significant blurs. Although Fig. 5 shows only partial visual results, the results are still representative. The quantitative PSNR results and visual results both indicate that the proposed method is effective in restoring blurred images from the Kohler image library. Although the processing objects are non-uniform blurred images, the proposed method still performs the task well.

**Qualitative Results.** The third group of experiments involved blind restorations of the representative eight degenerated images in the Lai image library. As shown in Fig. 6,

TABLE I: Average MSE Values for the Recovered Blur Kernels in the Levin Image Library.

Methods	Ker01	Ker02	Ker03	Ker04	Ker05	Ker06	Ker07	Ker08
Pan	$5.59 \times 10^{-2}$	$6.21 \times 10^{-2}$	$5.02 \times 10^{-2}$	$3.39 \times 10^{-2}$	$6.24 \times 10^{-2}$	$4.69 \times 10^{-2}$	$4.77 \times 10^{-2}$	$4.04 \times 10^{-2}$
Yan	$3.40 \times 10^{-2}$	$4.55 \times 10^{-2}$	$4.11 \times 10^{-2}$	$1.99 \times 10^{-2}$	$4.26 \times 10^{-2}$	$2.07 \times 10^{-2}$	$1.31 \times 10^{-2}$	$1.67 \times 10^{-2}$
Proposed	$9.71 \times 10^{-3}$	$8.93 \times 10^{-3}$	$9.42 \times 10^{-3}$	$3.84 \times 10^{-3}$	$2.92 \times 10^{-3}$	$1.28 \times 10^{-3}$	$7.75 \times 10^{-3}$	$4.85 \times 10^{-3}$

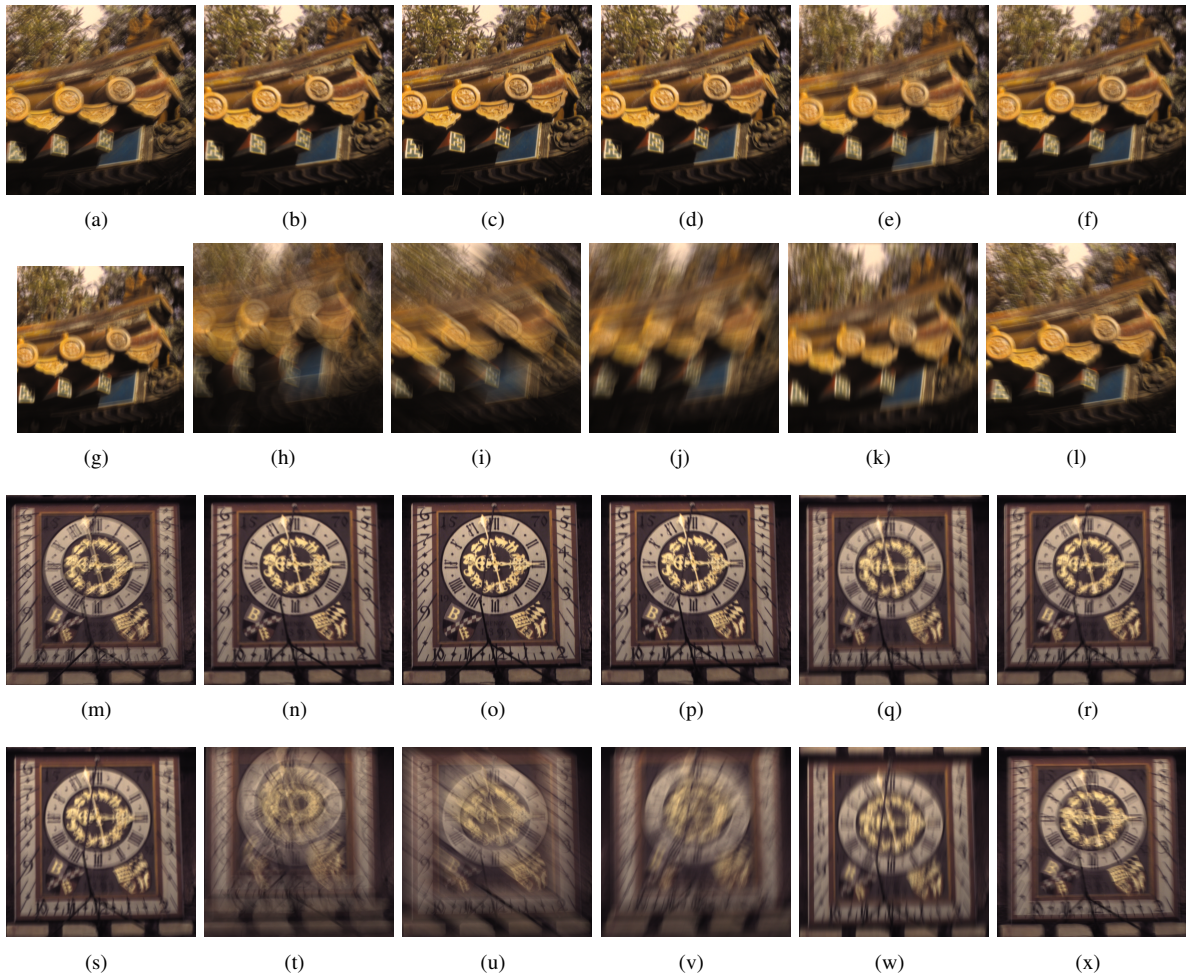


Fig. 4: Blurred Images from the Kohler Image Library.

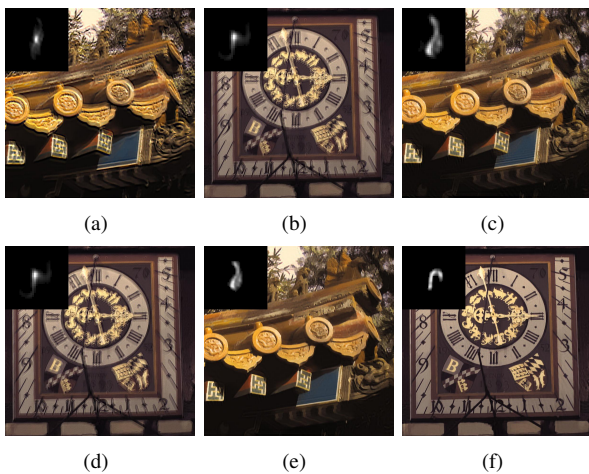


Fig. 5: Visual Results by Restoring Fig. 4(f) and Fig. 4(s). (a)-(b) Results of Pan's Method, (c)-(d) Results of Yan's Method, and (e)-(f) Results of the Proposed Method

the resolution, structural features, and degradation degrees of the eight blurred images are all different. Because the images in the library are blurred images collected from the real world, there are no original clear images, and the quality of the restoration results cannot be quantitatively analyzed. Most existing research qualitatively evaluates the restoration results of blurred images based on the corresponding visual effects (e.g., sharpness, brightness, artifacts, etc.). The experimental results for the three methods are shown in Figs. 7 to 10, where subfigures (a)-(b) are the results using Pan's method, subfigures (c)-(d) are the results using Yan's method, and subfigures (e)-(f) are the results using the proposed method. In general, the clear image reconstructed by Pan's method contains more artifacts than the images produced by the other methods. Notably, some artifacts are very obvious, as shown in Fig. 9(b), because Pan's method is most appropriate for relatively sparse text images. Therefore, the method is inclined to provide sparse solutions. However, there are few sparse real-world images. The blur estimation results based on Yan's method indicate that the



Fig. 6: Real-world Blurred Images from the Lai Image Library.

prior model used is likely to produce a relatively smooth solution. Therefore, the reconstructed image is relatively smooth. Typically, the blur of the image does not seem to be alleviated, as shown in Fig. 8(c). Among the three blind image restoration methods, the images reconstructed by the proposed method display the best visual effect. The blur removal in the reconstructed images is relatively thorough, and the images are therefore clearer, containing relatively few artifacts and retaining important details.

### V. CONCLUSION

A blind image restoration method based on sparse regularization is proposed in this paper. This method divides blind image restoration into two stages: blur estimation and clear image reconstruction. In the first stage, a new  $l_1 - l_2$  regularization optimization model is established, and the model is effectively processed to obtain an accurate estimation of the blur. In the second stage, the results of blur estimation are applied to image deconvolution, and the hyper-Laplacian prior method is used to complete clear image

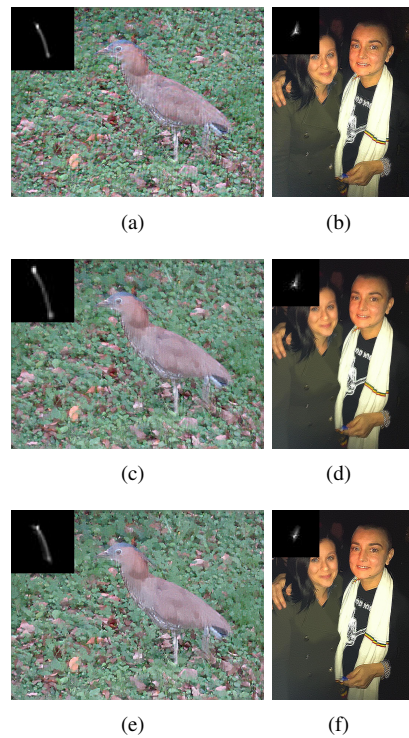


Fig. 7: Recovery Results for the Images Presented in Figs. 6(a) and 6(b). (a)-(b) Output of Pan's Method, (c)-(d) Output of Yan's Method, and (e)-(f) Output of the Proposed Method.

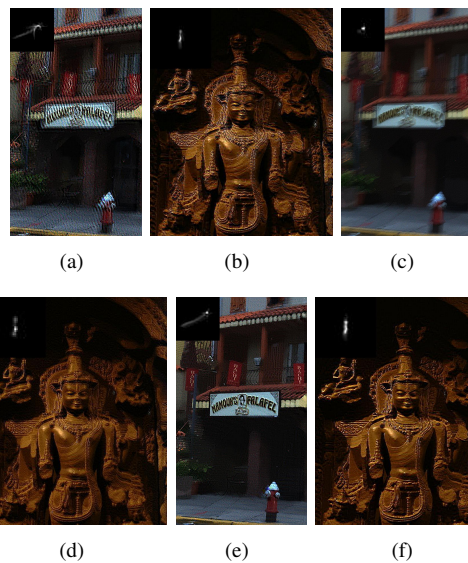


Fig. 8: Recovery Results for the Images Presented in Figs. 6(c) and 6(d). (a)-(b) Output of Pan's Method, (c)-(d) Output of Yan's Method, and (e)-(f) Output of the Proposed Method.

reconstruction. Experiments are performed by using three methods, including two methods for comparative purposes and the proposed method. The experimental objects are well-known standard test images from public image libraries. We perform restoration experiments on the blurred images of different color types and different blur types. The results of the methods are compared based on objective criteria and visual effects. The effectiveness of the proposed method is validated, and the advantages of this method over the other two methods are demonstrated.

TABLE II: PSNR Values (dB) for the Recovered Figs. 4(a)-(l).

Methods	Fig4a	Fig4b	Fig4c	Fig4d	Fig4e	Fig4f	Fig4g	Fig4h	Fig4i	Fig4j	Fig4k	Fig4l
Pan	30.60	30.40	32.67	32.68	32.76	30.69	30.64	33.73	31.37	33.48	32.07	32.46
Yan	29.84	29.90	32.42	31.98	32.94	28.97	30.21	33.41	31.89	32.88	31.24	32.56
Proposed	31.10	31.15	33.44	32.92	33.20	31.20	30.73	33.36	32.17	33.09	32.16	32.56

TABLE III: PSNR Values (dB) for the Recovered Figs. 4(m)-(x).

Methods	Fig4m	Fig4n	Fig4o	Fig4p	Fig4q	Fig4r	Fig4s	Fig4t	Fig4u	Fig4v	Fig4w	Fig4x
Pan	32.21	32.23	31.01	33.03	33.46	30.97	30.41	33.90	32.23	32.69	34.16	33.50
Yan	32.02	31.94	30.74	32.45	32.83	30.49	28.82	33.56	32.70	33.06	33.39	32.63
Proposed	33.03	32.39	31.12	33.34	33.63	31.66	29.85	35.92	33.78	34.08	34.17	33.68

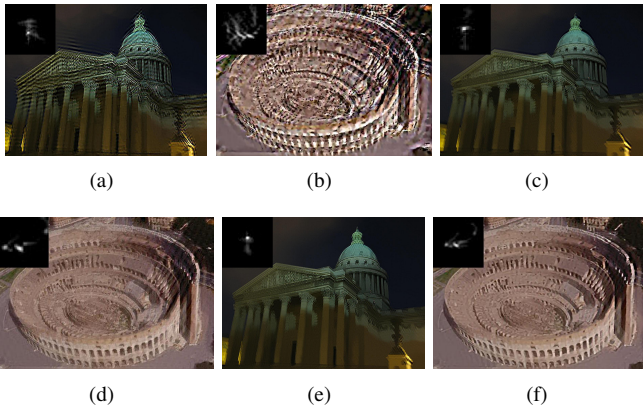


Fig. 9: Recovery Results for the Images Presented in Figs. 6(e) and 6(f). (a)-(b) Output of Pan's Method, (c)-(d) Output of Yan's Method, and (e)-(f) Output of the Proposed Method.

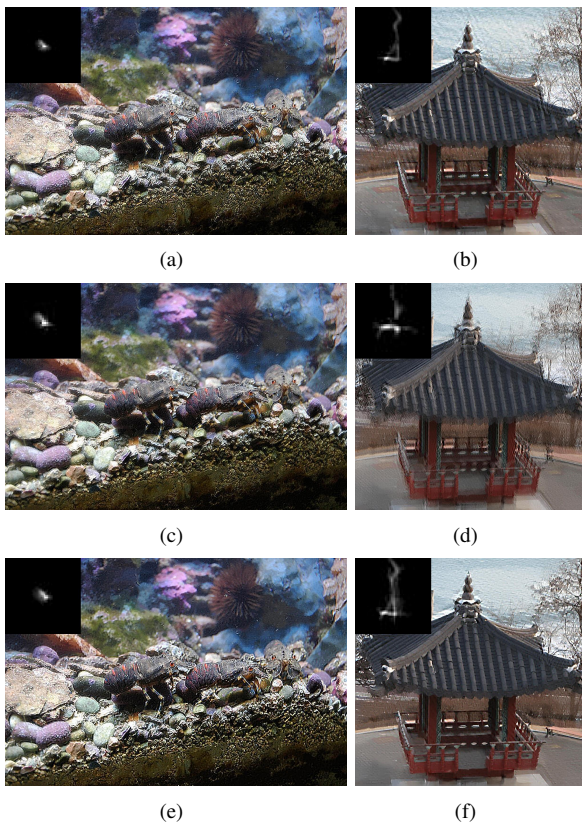


Fig. 10: Recovery Results for the Images Presented in Figs. 6(g) and 6(h). (a)-(b) Output of Pan's Method, (c)-(d) Output of Yan's Method, and (e)-(f) Output of the Proposed Method.

REFERENCES

- [1] S. D. Babacan, R. Molina, M. N. Do and A. K. Katsaggelos, "Bayesian Blind Deconvolution with General Sparse Image Priors," in 12th European Conference on Computer Vision 2012, pp. 341-355.
- [2] B. Amizic, R. Molina and A. K. Katsaggelos, "Sparse Bayesian Blind Image Deconvolution with Parameter Estimation," EURASIP Journal on Image and Video Processing, vol. 2012, no. 1, pp. 1-15, Dec. 2012.
- [3] W. Li, Q. Li, W. Gong and S. Tang, "Total Variation Blind Deconvolution Employing Split Bregman Iteration," Journal of Visual Communication and Image Representation, vol. 23, no. 3, pp. 409-417, Apr. 2012.
- [4] H. Zhang and D. Wipf, "Non-uniform Camera Shake Removal Using a Spatially-adaptive Sparse Penalty," in the 26th International Conference on Neural Information Processing Systems 2013, pp. 1556-1564.
- [5] L. Xu, S. Zheng and Jia Jiaya, "Unnatural  $L_0$  Sparse Representation for Natural Image Deblurring," in 2013 IEEE Conference on Computer Vision and Pattern Recognition 2013, pp. 1107-1114.
- [6] W. Zuo, D. Ren, D. Zhang, S. Gu and L. Zhang, "Learning Iteration-wise Generalized Shrinkage-thresholding Operators for Blind Deconvolution," IEEE Transactions on Image Processing, vol. 25, no. 4, pp. 1751-1764, Apr. 2016.
- [7] J. Cai, H. Ji, C. Liu and Z. Shen, "Framelet-based Blind Motion Deblurring from a Single Image," IEEE Transactions on Image Processing, vol. 21, no. 2, pp. 562-572, Feb. 2012.
- [8] J. Pan, Z. Hu, Z. Su and M. Yang, "Deblurring Text Images via  $L_0$ -regularized Intensity and Gradient Prior," in the IEEE Conference on Computer Vision and Pattern Recognition 2014, pp. 2901-2908.
- [9] W. Shao, H. Li, M. Elad, "Bi- $l_0$ - $l_2$ -norm Regularization for Blind Motion Deblurring," Journal of Visual Communication and Image Representation, vol. 33, pp. 42-59, Nov. 2015.
- [10] Y. Yan, W. Ren, Y. Guo, R. Wang and X. Cao, "Image Deblurring via Extreme Channels Prior," in IEEE Conference on Computer Vision and Pattern Recognition 2017, pp. 4003-4011.
- [11] D. Krishnan and R. Fergus, "Fast Image Deconvolution Using Hyper-Laplacian Priors," in 23rd Annual Conference on Neural Information Processing Systems 2009, pp. 1-9.
- [12] S. Cho and S. Lee, "Fast Motion Deblurring," ACM Transactions on Graphics, vol. 28, no. 5, pp. 1-8, Dec. 2009.
- [13] R. N. Bracewell, The Fourier Transform & Its Applications. New York: McGraw-Hill, 1999.
- [14] R. Fergus, B. Singh, A. Hertzmann, S. T. Roweis and W. T. Freeman, "Removing Camera Shake from a Single Photograph," ACM Transactions on Graphics, vol. 25, no. 3, pp. 787-794, Jul. 2006.
- [15] S. J. Wright, R. D. Nowak and M. A. T. Figueiredo, "Sparse Reconstruction by Separable Approximation," IEEE Transactions on Signal Processing, vol. 57, no. 7, pp. 2479-2493, Jul. 2009.
- [16] A. Levin, Y. Weiss, F. Durand and W. T. Freeman, "Understanding Blind Deconvolution Algorithms," IEEE Transactions on Pattern Analysis and Machine Intelligence, vol. 33, no. 12, pp. 2354-2367, Dec. 2011.
- [17] W. Kohler, M. Hirsch, B. Mohler, B. Scholkopf and S. Harmeling, "Recording and Playback of Camera Shake: Benchmarking Blind Deconvolution with a Real-World Database," in the 12th European Conference on Computer Vision 2012, pp. 27-40.
- [18] W. Lai, J. Huang, Z. Hu, N. Ahuja and M. Yang, "A Comparative Study for Single Image Blind Deblurring," in the 29th IEEE Conference on Computer Vision and Pattern Recognition 2016, pp. 1701-1709.